First Cold Spraying of Carbonated Biomimetic Nanocrystalline Apatite on Ti6Al4V: Physical–Chemical, Microstructural, and Preliminary Mechanical Characterizations

By *Emmanuelle Kergourlay, David Grossin,* Nuria Cinca, Claudie Josse, Sergi Dosta, Ghislaine Bertrand, Irene Garcia, Jose Maria Guilemany* and *Christian Rey*

Carbonated Biomimetic Nanocrystalline Apatite (BNAc) coatings are obtained for the first time by Cold Spray. The coatings are characterized by FTIR, Raman, XRD, and SEM and compared to the powders. No significant chemical and structural changes are detected and the nanostructure features of these very reactive BNAc are preserved in the coating. These results and preliminary mechanical assays show that Cold Spray can produce an operational biomimetic coatings offering a high potential for implants functionalization and osseointegration. However, these first results need further studies in order to understand the mechanism of adhesion and the interactions at the coating–substrate interface.

Hydroxyapatite $Ca_{10}(PO_4)_6(OH)_2$ coatings deposited on metallic implants by atmospheric plasma spray (APS) might now be considered the industrial standard.[1] These calcium phosphate coatings, which mimic bone mineral, have been found to enhance short and long-term osteointegration.[2]

However, two major criticisms with this type of coating need to be addressed:

Plasma spray is a process by which powder is melted and quenched in a few milliseconds. Such a thermal treatment results in an unavoidable degree of material degradation during processing (deshydroxylation, amorphization, etc),[3–5] limiting the long-term patency of coated implants.[6] Amorphization at the interface between metal and coating may lead to high rates of dissolution in body fluids at the point of interface, inducing a loss of coating adhesion.

Hydroxyapatite has a chemical composition and crystal characteristics very different from those of bone apatites.[7]

Natural bone mineral is a calcium phosphate nanocrystalline apatite which exhibits:[8] i) ionic vacancies in calcium and hydroxide crystal sites;[9] ii) substitution of calcium ions by a series of elements (present as minor elements like magnesium, or trace elements like strontium, etc.); and most importantly, iii) the replacement of PO_4^{3-} by divalent ions,[10] such as hydrogenophosphate HPO_4^{2-} or carbonate CO_3^{2-} ions.[11–12] It is estimated that almost a third of all PO_4^{3-} ions are replaced by HPO_4^{2-} and CO_3^{2-} bivalent species. Natural bone mineral is also characterized by platelet-shaped nanosized apatite crystals exhibiting a hydrated surface layer containing bivalent labile ions, offering a basis for functionalization with bioactive mineral ions or active molecules.[13,14] Synthesis and processing of biomimetic apatites for bone replacement have been the subject of numerous research activities due to their potent biological properties.[7] It is noteworthy that their physico-chemical features are highly dependent on the synthesis protocol and processing conditions.[15] Temperature is critical parameter in the processing of biomimetic

[*] *Dr. D. Grossin, Eng. E. Kergourlay, Dr. C. Josse, Prof. G. Bertrand, Prof. C. Rey*
Université de Toulouse, CIRIMAT, UMR 5085 INPT-CNRS-UPS, ENSIACET, 4 allée Emile Monso 31030 Toulouse, France
E-mail: david.grossin@ensiacet.fr
Dr. C. Josse
Centre de Microcaractérisation Raimond Castaing, UMS 3623, Espace Clément Ader, 3 rue Caroline Aigle, 31000 Toulouse, France
Dr. N. Cinca, Dr. S. Dosta, Dr. I. Garcia, Prof. J. M. Guilemany
Thermal Spray Centre (CPT), Universitat de Barcelona, Martí i Franqués, 1, 08028 Barcelona, Spain

nanocrystalline apatites. Soft processing conditions are required to preserve the hydrated layer the nanocrystalline dimensions, and prevent decomposition.[10,13,16] Several processes, using mostly wet-chemical techniques, have been described, such as dip coating, electrodeposition, electrophoretic deposition, and immersion in supersaturated solutions.[17] Additionally, physical deposition techniques, such as MAPLE,[18] have also been explored.

The above-cited contributions report promising results concerning the use of bone-like apatites in the field of biomaterials and have opened the way for a number of possibility in the coating industry. However, such coatings currently lack the mechanical properties required for biomedical applications.[1,19–20] These poor mechanical properties have led to the application of additional thermal treatments which can effectively increase adhesion strength, but may result in a loss of biological activity of the deposited materials.[21,22]

In this study, an industrial and relatively low-temperature thermal process, cold spraying (CS),[23] was investigated to obtain a coating of carbonated biomimetic nanocrystalline apatite BNAc on Ti6Al4V samples. Using this process, the particles are not melted, consequently, most of the initial characteristics of the particles, such as their chemical composition or the crystal size and habit,[24] are expected to be maintained.

Until now, the only published reports concerning the deposition of calcium phosphate apatites by CS involved stoichiometric HA or HA mixed with other compound onto metallic substrates or non-metallic substrates[25–31] Other reports have also been published on process modifications (e.g., substrate heating, ultrasonic powder feeding systems, etc.), and at least one modelling study of HA CS.[32–35] However, to the best of our knowledge, no reports of biomimetic nanocrystalline apatites cold sprayed onto Ti6Al4V, Co–Cr alloys, or stainless steel 316L have been published for use in medical applications. The present contribution is focused on the i) physical–chemical characterization of the BNAc coatings obtained via CS; ii) microstructure description; and iii) preliminary mechanical evaluation.

1. Results and Discussions

Raw BNAc powder and BNAc cold sprayed coatings are described in the experimental part of this paper. These are reproducible samples obtained after optimization of CS parameters.

X-ray diffraction analysis was conducted on the BNAc powder and on the scraped and ground BNAc coating, and compared to those of bone and stoichiometric HA (Figure 1). These diffraction patterns can be indexed in the apatitic structure (hexagonal, P63/m space group, ICDD PDF card 9-432).[36] In addition, no trace of impurity or secondary crystalline phases were detected in the coatings.

The poor crystallinity and/or the nanometric dimensions of the coating and the powder's crystals are evidenced by

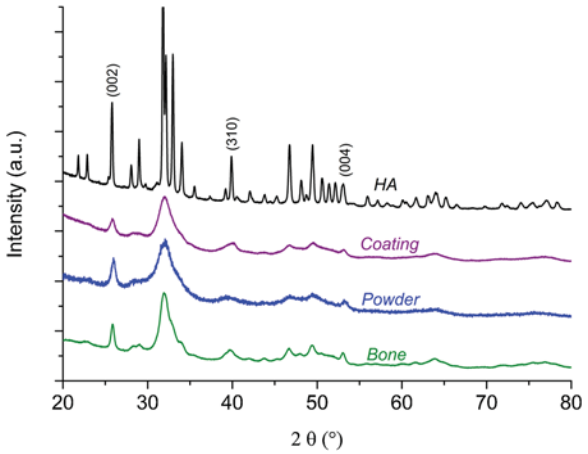

Fig. 1. XRD pattern of BNAc coating obtained by cold spray, BNAc powder, human bone,[54] and stoichiometric HA.

the width of the diffraction peaks in Figure 1. A similar observation was made in regard to the SPS processing of BNA in previous studies.[37] This is a specific feature of biological apatites found in bone (Figure 1).[13]

Profile fitting analysis allowed for the estimation of the unit cell parameters and crystallite size of the BNAc powder and coating (Table 1). Powder and coating cell parameters almost identical; for the "a" dimension, the difference corresponds to the standard deviation, and for the "c" dimension, the difference is about 0.1%. According to the literature, the widths of the peaks depends on the crystallographic orientation,[38] which alludes to the anisotropy of grain size (peaks (002) (004) appear narrower than (hk0) peaks). After CS, a small increase in crystallite size was noted, although the overall nanometer dimensions of the crystals were preserved.

The FTIR spectrum of the powder (Figure 2) shows the characteristic absorption bands of carbonated non-stoichiometric nanocrystalline apatite with:[36] i) rather poorly resolved phosphate bands at 472 cm^{-1} (ν_2 PO_4^{3-}), 563–603 cm^{-1} (ν_4 PO_4^{3-}), 961 cm^{-1} (ν_1 PO_4^{3-}), 1 030 and 1 081 cm^{-1} (ν_3 PO_4^{3-}), 873, 1 140–1 150, 1 250 cm^{-1}

Table 1. XRD results after pattern matching analysis.

XRD	Powder[a)]	Coating[a)]
a [Å]	9.449(2)	9.4496(13)
c [Å]	6.8951(17)	6.8883(10)
V[Å^3]	533.2(2)	532.68(13)
Rp [%]	2.18	2.47
Rwp [%]	2.83	3.19
GOF	1.06	1.11
FWHM(002)	0.5981	0.4973
FWHM(310)	2.5860	1.4586
L(002) nm[b)]	14(2)	17(2)
L(310) nm[b)]	3.4(3)	6.0(3)

[a)] see experimental part; [b)]using Scherrer approximation[58]

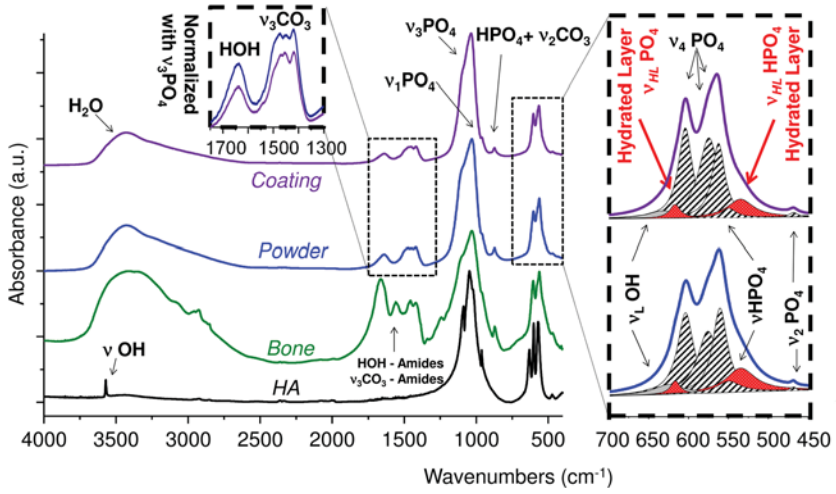

Fig. 2. FTIR of BNAc coating obtained by cold spray, BNAc powder, bone,[55] and stoichiometric HA; lateral insert: deconvolution from 450 to 700 cm^{-1} and front insert: normalized view (height of ν_3PO_4) from 1 300 to 1 750 cm^{-1}.

(HPO_4^{2-});[39] ii) the absence of sharp/intense OH^- bands at 630 cm^{-1} (OH^- libration) and 3 570 cm^{-1} (OH– elongation);[40] iii) relatively weak carbonate bands at 873 cm^{-1} (ν_2 CO_3^{2-}, superimposed to the HPO_4 broad line) and 1 350–1 550 cm^{-1} (ν_3 CO_3^{2-});[41] iv) water bands at 3 000–3 400 cm^{-1} and 1 637 cm^{-1}.[42] The FTIR spectrum of the coating was found to be very similar to the spectrum of the powder (Figure 2). Special attention was given to the absorption domain corresponding to the ν_4 PO_4^{3-} vibration mode. Indeed, this region was shown in earlier studies to include additional phosphate bands which were assigned to non-apatitic chemical environments (not present in well-crystallized stoichiometric HA).[42] These non-apatitic environments are related to the presence of a hydrated layer on the surface of the bone mineral or biomimetic nanocrystals.[12] This hydrated layer is thought to play a key role in the biological activity of apatite-based materials.[8] The characteristic broad shoulders at 500–550 cm^{-1} in the samples can be attributed to HPO_4^{2-}non-apatitic ions associated with a hydrated surface layer on the nanocrystals.[43] The most important difference between the powder and the coating FTIR spectra was a decrease of the absorption intensity in the 1 350–1 550 cm^{-1} domain attributed to the vibrations of carbonate ions. This phenomenon corresponds to the ≈12% reduction of ratio Area ($\nu_3CO_3^{2-}$):Area ($\nu_1\nu_3PO_4^{3-}$), calculated by integration. These observations reveal some slight modifications in the composition of the apatite nanocrystals.

The microstructure of selected samples was investigated by Scanning Electron Microscopy (SEM). A macroview, micrograph of the surface, cross-section view of the coating are shown in Figure 3. In the macroview, the uniform white color of the coated coupon highlights the homogeneity of the coating at this scale. The observation of grains was difficult, however, no apparent modification of the grain shape (rice-like morphology) on the surface of the coatings was observed.

Several methods can be used to determine the adherence of a coating.[44] The adherence of hydroxyapatite coatings is commonly measured by a standardized tensile test (ASTM C633-01, ISO 13779-4). In such testing, the thickness of the coating must be greater than 70 μm and thermal glue is used. Because CS coatings have a thickness in the order of 60 ± 10 μm and are thermal sensitive, this technique is not appropriate. Consequently, an alternative mechanical technique was implemented: the scratch test.[45,46] The critical load of BNAc cold sprayed and hydroxyapatite plasma sprayed coatings were 7 ± 2 and 11 ± 2 N, respectively.[47,48] The average roughness (Ra) of both coatings was in the same range (4 ± 0.2 μm and 7.2 ± 0.6 μm, respectively), whereas the thickness was quite different (60 ± 10 μm and 85 ± 8 μm respectively), which might explain these differences in critical load.[49]

2. Conclusion

In conclusion, the cold sprayed coatings exhibited grain-shape and nanosized crystals similar to the biomimetic BNAc powder. The chemical composition and crystalline phase were also maintained. Moreover, the labile ion-containing

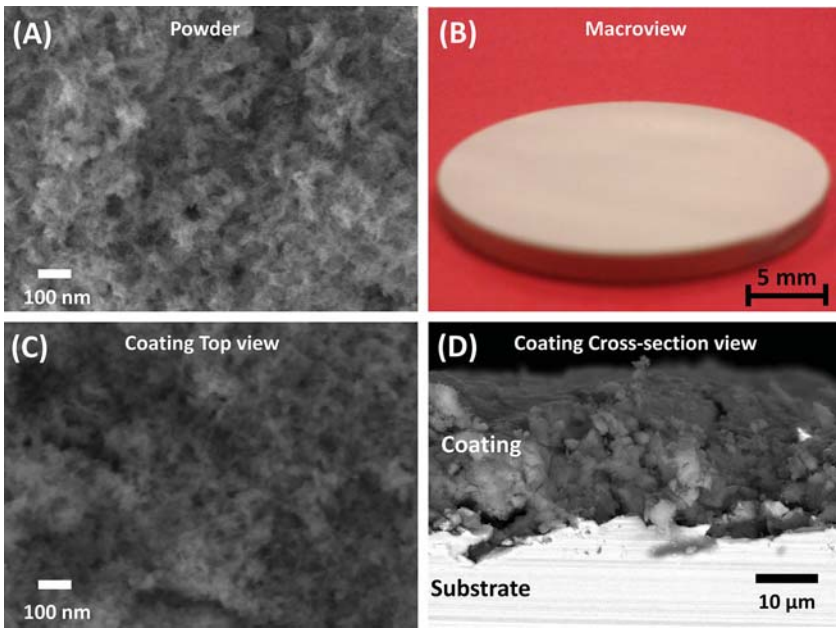

Fig. 3. (A) SEM micrograph of powder, (B) coated material macroview, (C) SEM micrograph of coated material (top view), and (D) SEM micrograph of cross-section of coated material.

hydrated layer was preserved, thereby allowing for greater biological activity as compared to plasma sprayed hydroxyapatite coatings. On top of its ability to maintain the physical–chemical and microstructural characteristics of thermal sensitive apatite, CS permits the production of coatings with sufficient adhesion to be applied to medical implants.

3. Experimental Section

3.1. Synthesis of BNAc Powder

A synthesis[36] of carbonated biomimetic nanocrystalline apatite (BNAc) was obtained by precipitation in aqueous medium at close-to-physiological pH and room temperature. Precipitation involved separate sources for calcium ions, and phosphate and carbonate ions. The each solution was prepared in advance of precipitation. The calcium solution (solution A, typically 1 500 ml) was prepared by dissolving calcium nitrate $Ca(NO_3)_2 \cdot 4H_2O$ (Merck Emsure grade, purity $\geq 99.0\%$) in deionized water up to a concentration of 0.3 M. A solution containing phosphate and carbonate (solution B, typically 3 000 ml) was prepared by dissolving di-ammonium hydrogenphosphate $(NH_4)_2HPO_4$ (VWR Normapur grade, purity $\geq 99.0\%$) and sodium hydrogencarbonate $NaHCO_3$ (Carlo Erba analytical grade, purity $\geq 99.0\%$) up to the respective concentrations of 0.45 and 0.71 M. Solution A was rapidly poured into stirred solution B, then left to mature in the precipitating medium for 1 day (ageing in solution) at room temperature (20–25 °C). During this synthesis, the reaction medium was buffered at a pH value close to physiological pH (pH ≈ 7.2) by the presence of excess phosphate and carbonate ions. The precipitating medium was then separated into four equal parts, filtered through Büchner funnels, thoroughly washed with deionized water (4 L per funnel), and freeze-dried for 3 days (freeze-dryer set between −60 and −80 °C, residual pressure 10–12 mbar). Unless otherwise stated, the freeze-dried precipitate powder was then collected and stored in a freezer at −18 °C prior to physico-chemical analysis.

3.2. Titanium Alloy Substrate Preparation

Commercial Ti6Al4V ELI (Harald Pihl, Sweden) disks (25 mm × 2 mm) were used as substrates for this study. The samples were subjected to different surface treatments before deposition: i) degreasing by immersion in acetone followed by rinsing with demineralized water; ii) pickling in a commercial solution (DBP Mayet, France) composed of a mixture of fluorhydric acid ($0 < wt\% < 1$) and nitric acid ($2.5 < wt\% < 10$) for 2 min followed by rinsing under tap water then demineralized water; and iii) passivation in a nitric acid solution (46 wt %) for 30 min followed by rinsing in tap water then demineralized water. The three aqueous treatments were prepared at room temperature, without stirring, and the samples were air-dried between treatments. To finish, samples were sandblasted using the CS process with alumina particles before deposition with BNAc.

3.3. Cold Spray Process

The deposition of BNAc was performed at the Thermal Spray Centre (Barcelona, Spain) using a LPCS "low pressure cold spray" system, Dymet 423, equipped with a de Laval nozzle (converging-diverging nozzle). The BNAc powder was injected via a vibrated powder feeder into pure heated air used as accelerating and carrier gas. The gas pressure was set between 0.5 and 0.9 MPa and the temperature was varied from RT to 500 °C. The spray distance and the traversing speed were fixed to produce homogeneous coatings with thickness ranging from 10 to 60 μm.

3.4. X-Ray Diffraction

X-ray diffraction analysis was performed on the coatings using a Bruker D8-2 diffractometer (Cu, Kα1, and Kα2 radiation). The nature and crystallographic features of the crystalline phases were evaluated according to international standards (ISO 13779-3:08). The counting time was 3 s for every 0.02° step, typically in the range 2θ [20–80°]. JANA2006 software allowed for the evaluation of unit cell parameters and volume using Pseudo-Voigt profile function and anisotropic particle broadening.[50] The full-width at half-maximum (FWHM) was extracted after profile fitting. The Scherrer approximation was used to estimate coherence length and to extrapolate crystallite size.[51–53] The XRD of human mineral bone comes from the work of Grunenwald et al. (femur, male, 57 years old).[54]

3.5. Spectroscopic Analysis

Fourier Transform Infrared (FTIR) spectra of the removed and ground coatings were obtained using a Nicolet 5700 spectrometer in the 400–4 000 cm^{-1} range (64 scans, resolution 4 cm^{-1}). Spectral decomposition was performed after subtracting a linear baseline in the 400–800 cm^{-1} wavenumber range corresponding to the ν_2, ν_4 (PO_4) and ν (OH) vibration modes of phosphate and hydroxide ions using ORIGIN (version 8.6) software.[40] The FTIR spectra of bone come from the work of Bohic et al.[55]

3.6. SEM

The coatings microstructure was characterized by SEM FEG (Jeol JSM-7100F TTLS LV) at the Centre of Microcharacterization Raimond Castaing (Toulouse, France).

3.7. Mechanical Evaluation by Scratch Test

The scratch test was conducted to evaluate coating adhesion.[45,46,56,57] The deposited specimen (thickness 60 ± 10 μm) was scratched using "Revetest" (CSM Instrument) with a diamond Rockwell indenter of 200 μm in diameter and a pre-load of 1 N, load speed 15 N min^{-1}, scratch speed 1.5 mm min^{-1}, and a maximum load of 50 N.

[1] L. M. Sun, C. C. Berndt, K. A. Gross, A. Kucuk, *J. Biomed. Mater. Res.* **2001**, *58*, 570.
[2] K. Degroot, R. Geesink, C. Klein, P. Serekian, *J. Biomed. Mater. Res.* **1987**, *21*, 1375.
[3] R. B. Heimann, *Surf. Coat. Technol.* **2006**, *201*, 2012.
[4] M. T. Carayon, J. L. Lacout, *J. Solid State Chem.* **2003**, *172*, 339.
[5] R. B. Heimann, R. Wirth, *Biomaterials* **2006**, *27*, 823.
[6] I. Demnati, D. Grossin, C. Combes, C. Rey, *J. Med. Biol. Eng.* **2014**, *34*, 1.
[7] C. Combes, C. Rey, *Actual. Chim.* **2003**, 16.
[8] C. Rey, C. Combes, C. Drouet, M. J. Glimcher, *Osteoporos. Int.* **2009**, *20*, 1013.
[9] C. Rey, J. L. Miquel, L. Facchini, A. P. Legrand, M. J. Glimcher, *Bone* **1995**, *16*, 583.
[10] S. Cazalbou, C. Combes, D. Eichert, C. Rey, *J. Mater. Chem.* **2004**, *14*, 2148.

[11] L. T. Kuhn, M. D. Grynpas, C. C. Rey, Y. Wu, J. L. Ackerman, M. J. Glimcher, *Calcif. Tissue Int*. **2008**, *83*, 146.
[12] C. Rey, B. Collins, T. Goehl, I. R. Dickson, M. J. Glimcher, *Calcif. Tissue Int*. **1989**, *45*, 157.
[13] H. M. Kim, C. Rey, M. J. Glimcher, *Calcif. Tissue Int*. **1996**, *59*, 58.
[14] C. Rey, E. Strawich, M. J. Glimcher, *Bull. Inst. Oceanogr. Monaco* **1994**, 55.
[15] C. Drouet, *BioMed Res. Int*. **2013**, *2013*, 490946.
[16] C. Rey, C. Combes, *BoneKEy Rep*. **2014**, *3*, 586.
[17] P. Habibovic, F. Barrère, C. A. Van Blitterswijk, K. de Groot, P. Layrolle, *J. Am. Ceram. Soc*. **2002**, *85*, 517.
[18] A. Visan, D. Grossin, N. Stefan, L. Duta, F. M. Miroiu, G. E. Stan, M. Sopronyi, C. Luculescu, M. Freche, O. Marsan, C. Charvillat, S. Ciuca, I. N. Mihailescu, *Mater. Sci. Eng. B Adv. Funct. Solid State Mater.* **2014**, *181*, 56.
[19] E. Mohseni, E. Zalnezhad, A. R. Bushroa, *Int. J. Adhes. Adhes*. **2014**, *48*, 238.
[20] ISO 13779-4:2002(E), **2002**.
[21] F. Dabbarh, A. Lebugle, A. Taitai, M. Bennani, *Ann. Chim. Sci. Mater.* **2000**, *25*, 339.
[22] M. Bennani, A. Lebugle, G. Bonel, *Ann. Chim. Sci. Mater.* **1993**, *18*, 245.
[23] A. Papyrin, *Adv. Mater. Process*. **2001**, *159*, 49.
[24] F. Gartner, T. Stoltenhoff, T. Schmidt, H. Kreye, *J. Therm. Spray Technol*. **2006**, *15*, 223.
[25] X. Zhou, P. Mohanty, *Electrochimi. Acta* **2012**, *65*, 134.
[26] Y. Liu, J. Huang, H. Li, *J. Therm. Spray Technol*. **2014**, *23*, 1149.
[27] Y. Liu, Z. Dang, Y. Wang, J. Huang, H. Li, *Carbon* **2014**, *67*, 250.
[28] N. Sanpo, M. L. Tan, P. Cheang, K. A. Khor, *J. Therm. Spray Technol*. **2008**, *18*, 10.
[29] M. Gardon, A. Concustell, S. Dosta, N. Cinca, I. G. Cano, J. M. Guilemany, *Mater. Sci. Eng. C* **2014**, *45*, 117.
[30] A. C. W. Noorakma, H. Zuhailawati, V. Aishvarya, B. K. Dhindaw, *J. Mater. Eng. Perform*. **2013**, *22*, 2997.
[31] J. H. Lee, H. L. Jang, K. M. Lee, H.-R. Baek, K. Jin, K. S. Hong, J. H. Noh, H.-K. Lee, *Acta Biomater.* **2013**, *9*, 6177.
[32] L. Zhang, W. Zhang, Z. Wu, *Appl. Mech. Mater.* **2012**, *130*, 900.
[33] L. Zhang, W. Zhang, H. Li, W. Geng, Y. Bao, *Appl. Mech. Mater.* **2012**, *151*, 300.
[34] L. Zhang, W. T. Zhang, *Adv. Mater. Red*. **2011**, *188*, 717.
[35] R. P. Singh, U. Batra, *J. Appl. Fluid Mech*. **2013**, *6*, 555.
[36] S. Cazalbou, C. Combes, D. Eichert, C. Rey, M. J. Glimcher, *J. Bone Miner. Metab*. **2004**, *22*, 310.
[37] D. Grossin, S. Rollin-Martinet, C. Estournes, F. Rossignol, E. Champion, C. Combes, C. Rey, C. Geoffroy, C. Drouet, *Acta Biomater.* **2010**, *6*, 577.
[38] D. Grossin, M. Banu, S. Sarda, S. Martinet-Rollin, C. Drouet, C. Estournes, E. Champion, F. Rossignol, C. Combes, C. Rey, in *Adv. Bioceram. Porous Ceram. Ii* (Eds: R. Narayan, P. Colombo), John Wiley & Sons, Inc., Hoboken, USA **2010**, 113.
[39] D. Eichert, C. Combes, C. Drouet, C. Rey, in *Bioceram. Vol 17* (Eds: P. Li, K. Zhang, C.W. Colwell), Trans Tech Publications, Uetikon-Zuerich, Switzerland **2004**, 3
[40] C. Rey, C. Combes, C. Drouet, H. Sfihi, A. Barroug, *Mater. Sci. Eng. C Biomim. Supramol. Syst*. **2007**, *27*, 198.
[41] A. Grunenwald, C. Keyser, A. M. Sautereau, E. Crubézy, B. Ludes, C. Drouet, *J. Archaeol. Sci*. **2014**, *49*, 134.
[42] D. Eichert, H. Sfihi, C. Combes, C. Rey, in *Bioceram. Vol 16* (Eds: M.A. Barbosa, F.J. Monteiro, R. Correia, B. Leon), Trans Tech Publications, Uetikon-Zuerich, Switzerland **2004**, 927.
[43] D. Eichert, C. Drouet, H. Sfihi, C. Rey, C. Combes, in *Trends Biomater. Res*. (Ed: P. Pannone), Nova Science Publishers, Inc., New York, USA **2007**, 93.
[44] B. Ben-Nissan, B. A. Latella, A. Bendavid, in *Compr. Biomater.* (Ed: P. Ducheyne), Elsevier, Oxford **2011**, 63.
[45] A. Behnamghader, D. Najjar, A. Iost, S. Benayoun, in *Thermec 2009 Pts 1-4* (Eds: T. Chandra, N. Wanderka, W. Reimers, M. Ionescu), Trans Tech Publications Ltd, Stafa- Zurich **2010**, 641.
[46] A. J. Perry, *Thin Solid Films* **1981**, *78*, 77.
[47] I. Demnati, M. Parco, D. Grossin, I. Fagoaga, C. Drouet, G. Barykin, C. Combes, I. Braceras, S. Goncalves, C. Rey, *Surf. Coat. Technol*. **2012**, *206*, 2346.
[48] I. Demnati, D. Grossin, C. Combes, M. Parco, I. Braceras, C. Rey, *Biomed. Mater.* **2012**, *7*, 054101.
[49] I. Demnati, D. Grossin, O. Marsan, G. Bertrand, G. Collonges, C. Combes, M. Parco, I. Braceras, J. Alexis, Y. Balcaen, C. Rey, *Open Biomed. Eng. J*. **2015**, *9*, 26.
[50] V. Petricek, M. Dusek, L. Palatinus, *Z. Krist*. **2014**, *229*, 345.
[51] P. Scherrer, *Nachrichten Von Ges. Wiss. Zu Gött. Math. -Phys. Kl*. **1918**, *1918*, 98.
[52] A. L. Patterson, *Phys. Rev.* **1939**, *56*, 978.
[53] J. I. Langford, A. J. C. Wilson, *J. Appl. Crystallogr.* **1978**, *11*, 102.
[54] A. Grunenwald, C. Keyser, A. M. Sautereau, E. Crubezy, B. Ludes, C. Drouet, *Anal. Bioanal. Chem*. **2014**, *406*, 4691.
[55] S. Bohic, C. Rey, A. Legrand, H. Sfihi, R. Rohanizadeh, C. Martel, A. Barbier, G. Daculsi, *Bone* **2000**, *26*, 341.
[56] M. C. Kuo, S. K. Yen, *Mater. Sci. Eng. C* **2002**, *20*, 153.
[57] K. Cheng, C. Ren, W. Weng, P. Du, G. Shen, G. Han, S. Zhang, *Thin Solid Films* **2009**, *517*, 5361.
[58] J. I. Langford, A. J. C. Wilson, *J. Appl. Crystallogr.* **1978**, *11*, 102.